THE JOURNAL OF PHYSICAL CHEMISTRY C

Article

pubs.acs.org/JPCC

Active Control of SPR by Thermoresponsive Hydrogels for Biosensor Applications

Mana Toma,[†] Ulrich Jonas,[‡,§] Anca Mateescu,[§] Wolfgang Knoll,[†,∥] and Jakub Dostalek*[,†]

[†]AIT-Austrian Institute of Technology, BioSensor Technologies, Muthgasse 11/2, 1190 Vienna, Austria

[‡]Macromolecular Chemistry, University of Siegen, Department Chemistry-Biology, Adolf-Reichwein-Strasse 2, Siegen 57076, Germany

[§]Foundation for Research and Technology Hellas (FORTH), Bio-Organic Materials Chemistry Laboratory (BOMCLab), P.O. Box 1527, 71110 Heraklion, Crete, Greece

[∥]Nanyang Technological University, Centre for Biomimetic Sensor Science, Singapore 637553

Supporting Information

ABSTRACT: The use of thermoresponsive poly(*N*-isopropylacrylamide)-based hydrogel (pNIPAAm) for rapid tuning of surface plasmon resonance (SPR) is reported. This approach is implemented by using an SPR layer architecture with an embedded indium tin oxide microheater and pNIPAAm film on its top. It takes advantage of rapid thermally induced swelling and collapse of pNIPAAm that is accompanied by large refractive index changes and leads to high thermo-optical coefficient of $dn/dT = 2 \times 10^{-2}$ RIU/K. We show that this material is excellently suited for efficient control of refractive index-sensitive SPR and that it can serve simultaneously as a 3D binding matrix in biosensor applications (if modified with biomolecular recognition elements for a specific capture of target analyte). We demonstrate that this approach enables modulating of the output signal in surface plasmon-enhanced fluorescence spectroscopy biosensors and holds potential for simple time-multiplexing of sensing channels for parallelized readout of fluorescence assays.

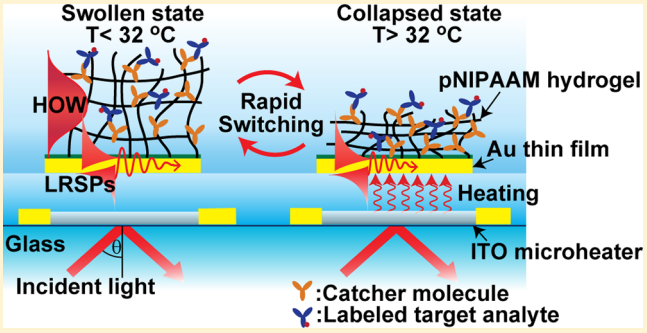

1. INTRODUCTION

Plasmonics represents a rapidly developing research and technology area that exploits the tight confinement of electromagnetic field associated with its coupling to surface plasmons—optical waves originating from collective oscillations of the electron plasma on surfaces of metallic nanostructures and thin films.[1] Fast and reversible tuning of surface plasmons is crucial to harness the potential of plasmonics in important areas such as signal processing, optical sensors, and biosensors. Up to now, the interfacing of metallic structures with dielectric materials for electro-optical,[2] thermo-optical,[3] magneto-optical,[4] photoinduced,[5] and electrochemical[6] -based modulating of refractive index was pursued for rapid tuning of surface plasmon resonance (SPR). However, these approaches typically allow for only weak refractive index changes ($<10^{-2}$ to 10^{-3})[7] that are not sufficient to control SPR efficiently.

Poly(*N*-isopropylacrylamide) (pNIPAAm) is an excellently suited alternative material for active control of SPR in the visible/near-infrared spectrum. It is a well-characterized thermoresponsive hydrogel with lower critical solution temperature (LCST) of 32 °C. Below the LCST, pNIPAAm exhibits a highly open, water-swollen structure, while above the LCST it collapses with a release of bound water, which leads to an increase in its density and correspondingly of the refractive index.[8] Thin pNIPAAm brush layers were recently reported for tuning of the localized surface plasmon resonance (LSPR) on arrays of metallic nanoparticles[9] and were applied in surface-enhanced Raman spectroscopy.[10] In addition, SPR on planar metallic surfaces was employed for the investigation of cross-linked pNIPAAm layers.[8,11] In our laboratory, various hydrogel materials derived from pNIPAAm were developed to serve as an extended 3D binding matrix in refractometric[12,13] and surface plasmon-enhanced fluorescence spectroscopy (SPFS)[14,15] biosensors for detection of trace amounts of molecular analytes. The equilibrium responsive properties of cross-linked pNIPAAm layers were extensively studied as a function of slow-temperature variations depending on the network density, solvent, and polymer backbone modifications.[8,16,17]

This paper extends these studies by investigating the kinetics of transition between the swollen and the collapsed state and its dependence on the postmodification by protein molecules. In addition, the implementation of pNIPAAm thermoresponsive binding matrix for rapid switching on and off the resonant

Received: January 9, 2013
Revised: April 27, 2013
Published: May 6, 2013

   dx.doi.org/10.1021/jp400255u | *J. Phys. Chem. C* 2013, 117, 11705−11712

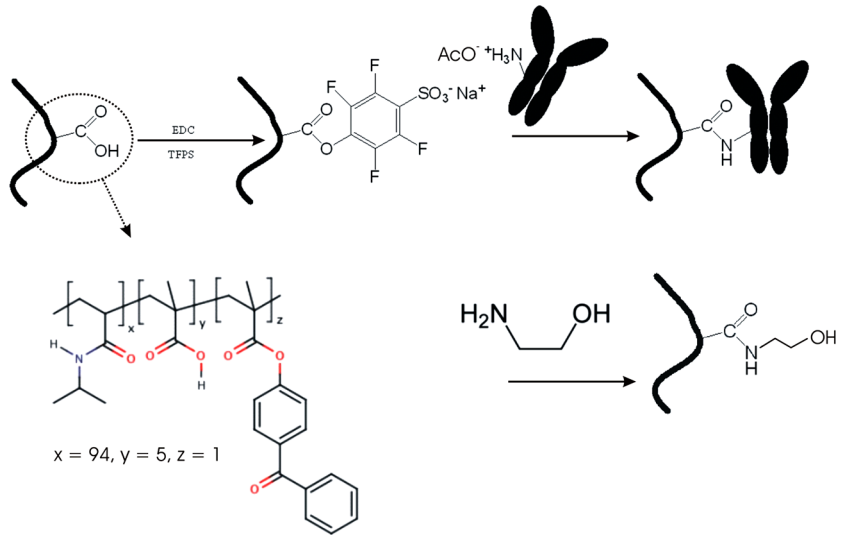

Figure 1. Schematics of photo-cross-linkable pNIPAAm hydrogel system and its modification with protein molecules by using amine coupling chemistry.

coupling to surface plasmons is demonstrated and utilized for modulating of fluorescence signal in an SPFS biosensor.

2. EXPERIMENTAL SECTION

2.1. Materials. Sodium *para*-tetrafluorophenol sulfonate (TFPS) and 3-(4-benzoylphenoxy)propanethiol (BP-thiol) were synthesized as described in the literature.[17,18] The Cytop fluoropolymer (CTL-809M) was purchased from Asahi Glass (Japan). SU-8 and its solvent were obtained from MicroChem (USA). Phosphate-buffered saline (PBS, 10 mM phosphate, 140 mM NaCl, 3 mM KCl and a pH of 7.4) was from Calbiochem (Germany). PBS-Tween buffer (PBST) was prepared by adding 0.05 vol % of Tween 20 to the PBS solution. 1-Ethyl-3-(3-dimethylaminopropyl)carbodiimide (EDC) was obtained from Pierce (USA). Ten mM acetate buffer (ACT with pH 4) was prepared from sodium acetate, and its pH was adjusted by adding acetic acid. An ethanolamine (ETA) was dissolved in water at the concentration of 1 M, and the pH was adjusted to 8.5 by adding sodium hydroxide. Mouse immunoglobulin G (mIgG) and goat antimouse IgG (a-mIgG) that was labeled with Alexa Fluor 647 were purchased from Molecular Probes (USA). All other chemicals were acquired from Sigma-Aldrich (Germany).

2.2. Polymer Synthesis. A random terpolymer composed of *N*-isopropylacrylamide (NIPAAm, 94% monomer concentration), methacrylic acid (MAA, 5% m.c.), and 4-benzophenonemethacrylate (BPMA, 1% m.c.) shown in Figure 1 was synthesized by free-radical polymerization in our laboratory, as described elsewhere.[19] The NIPAAm provided the thermoresponsive characteristics of the terpolymer, the benzophenone moieties enabled its photo-cross-linking, and the MAA allowed the postsynthetic modification with proteins.

2.3. Fabrication of Sensor Chip. First, a microheater that consists of 25 nm thick indium tin oxide (ITO) pad and a pair of 50 nm thick gold electrodes was prepared on a BK7 glass substrate by magnetron sputtering (UNIVEX 450C, Leybold, Germany). The ITO pad with area of 0.5 × 1 mm and the gold electrode stripes with width of 0.5 mm were defined by using a set of CO_2 laser-cut stencil masks. On top of the ITO microheater, a layer architecture supporting long-range surface plasmons (LRSPs) was deposited as described in previous works.[20,21] In brief, a Cytop fluoropolymer layer with a thickness of 600 nm was spincoated on the top of the ITO microheater, followed by the sputtering of a 20 nm thick SPR-active gold film. The Cytop film served as a low refractive index buffer layer as well as an insulator layer protecting the ITO microheater and gold electrodes. Because the refractive index of Cytop (n = 1.337 at the wavelength of λ = 633 nm) is close to that of water and hydrogels, it provides a refractive index symmetrical geometry that is required for the excitation of LRSPs on the thin gold film; see Figure 2. Let us note that

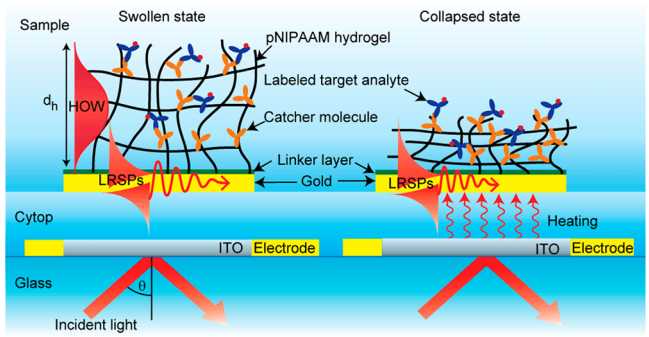

Figure 2. Sensor chip with embedded ITO microheater and SPR-active layer architecture on the top carrying a thermoresponsive pNIPAAm hydrogel layer.

LRSPs exhibit lower losses than regular surface plasmons. Therefore, their excitation is accompanied by narrower resonance that provides a higher figure of merit in refractometric measurements and is associated with a stronger field intensity, which is advantageous in various spectroscopy enhancement strategies.[20]

pNIPAAm-based hydrogel layer was tethered to a gold surface by using SU-8 or BP-thiol linker layers. The SU-8 layer with the thickness of 10 nm was prepared by spin-coating. Alternatively, the BP-thiol self-assembled monolayer (SAM) was formed by overnight incubating the gold surface in 1 mM BP-thiol solution in ethanol, followed by rinsing with pure ethanol and drying in a stream of nitrogen. Afterward, pNIPAAm-based polymer dissolved in ethanol at a concen-

dx.doi.org/10.1021/jp400255u | J. Phys. Chem. C 2013, 117, 11705−11712

tration of 20 mg/mL was spin-coated onto the surface. The polymer layer was dried in vacuum and exposed to UV light (irradiation dose of 4 J/cm^2 at a wavelength of λ = 365 nm) to covalently cross-link and attach the polymer network to the gold surface.

The thickness d_h and refractive index n_h of the swollen hydrogel film were probed by resonantly excited surface waves and determined by fitting respective reflectivity spectra by a Fresnel-based model, as described in more detail in the Supporting Information. This approach relies on the simultaneous excitation of surface waves probing the hydrogel-coated surface with different penetration depths. In particular, we took advantage of the fact that the hydrogel film can serve as a hydrogel optical waveguide (HOW) enabling the excitation of additional modes besides surface plasmons. A "box" approximation was used in which a potential gradient of the hydrogel density perpendicular to the surface was neglected.[12] A similar approach was used for the measurement of the thickness of a dry hydrogel film $d_{h\text{-}dry}$ in contact with air that exhibits a refractive index of $n_{h\text{-}dry}$ = 1.48.[14]

The post-modification of pNIPAAm-based polymer network by protein molecules (mIgG antibodies) was performed in situ by using the amine coupling. First, the MAA carboxylic moieties were activated by 20 min of incubation in an aqueous solution with a mixture of TFPS (21 mg/mL) and EDC (75 mg/mL). Then, the surface was rinsed with ACT buffer for 5 min and reacted with mIgG dissolved in ACT buffer at a concentration of 50 μg/mL. The surface mass density of covalently immobilized mIgG was varied from Γ = 0 to 27 ng/mm^2 (as observed from respective changes in the thickness d_h and refractive index n_h[5]) by adjusting the reaction time between 0 and 60 min. Finally, the unreacted TFPS moieties were blocked by 20 min of incubating in a 1 M ETA solution, followed by rinsing with PBS for 10 min.

2.4. Experimental Setup. An optical setup utilizing attenuated total reflection (ATR) method with the Kretschmann configuration was used. This setup combined the angular interrogation with spatially resolved measurements based on surface plasmon resonance imaging (SPRI). As shown in Figure 3, a parallel monochromatic light beam was coupled to a 90° LASFN9 glass prism. As a light source, He−Ne laser (SPT1, CVI Melles Griot, Germany) or LED (LE-1R-C, WT&T, Canada) emitting light at a wavelength of λ = 633 nm were used. Transverse magnetic (TM) polarization was selected using a polarizer, and a narrow transmission band-pass filter (FL632.8-10, Thorlabs) was used to block the light at wavelengths different from 633 nm. At the prism base, a sensor chip with the ITO microheater and the LRSP-supporting layers was optically matched by using a refractive index matching oil. The intensity of the light beam reflected from the prism base was measured with a photodiode connected to a lock-in amplifier (model 5210, Princeton Applied Research, USA) or by using a CCD camera (piA1000-48gm, Basler AG, Germany) with a C-mount camera lens (UNIFOC 58, Schneider Kreuznach, Germany). A two-circle rotation stage (Huber, Germany) was used for the control of the angle of incidence θ of a light beam hitting the gold sensor surface. For the kinetics measurement, the angle of incidence θ was fixed in the vicinity to the one at which LRSPs were resonantly excited, and the reflectivity signal R was measured as a function of time. In the fluorescence experiments, a surface wave was resonantly excited at the wavelength matching the absorption band of fluorophore labels $\lambda \approx \lambda_{ab}$ for the excitation of fluorescence light. The fluorescence light emitted at higher wavelength λ_{em} by fluorophore labels attached to affinity-captured molecules was collected through an aqueous medium by a lens (NA = 0.3). The peak absorption and emission wavelengths of used Alexa Fluor 647 labels were of λ_{ab} = 652 and λ_{em} = 670 nm, respectively. The intensity of fluorescence light at λ_{em} was measured in counts per second (cps) by a photomultiplier tube (H6240-01, Hamamatsu, Japan) that was connected to a counter (53131A, Agilent, USA). For spatially resolved fluorescence measurements, the photomultiplier tube was replaced by an electron-multiplying charge-coupled device (EM-CCD iXon+885, Andor Technology, Ireland). A set of filters including notch (XNF-632.8-25.0M, CVI Melles Griot, Germany) and band-pass (670FS10-25, LOT-Oriel, Germany) filters was used to suppress the background signal.

A flow cell with a volume of 25 μL was attached to the sensor surface to flow liquid samples at 0.5 mL/min by using a peristaltic pump. The sensor head comprising the prism, the sensor chip, and the flow cell was temperature-stabilized at a background temperature T_0 by a Peltier device connected to its driver (LFI3751, Wavelength Electronics, USA). To rapidly heat the sensor surface, we connected the ITO microheater with a typical resistance of 280 Ω to a current modulator (NI9265, National Instruments, USA) via the gold electrodes. The data acquisition, image processing, and control of the overall sensor system were performed by using home-developed LabVIEW-based software. Local temperature changes induced by the current flow through an ITO microheater I were optically calibrated, and the characteristic response time was determined as δt_μ = 50 ms. (More detailed information is provided in the Supporting Information; see Figure S1a.)

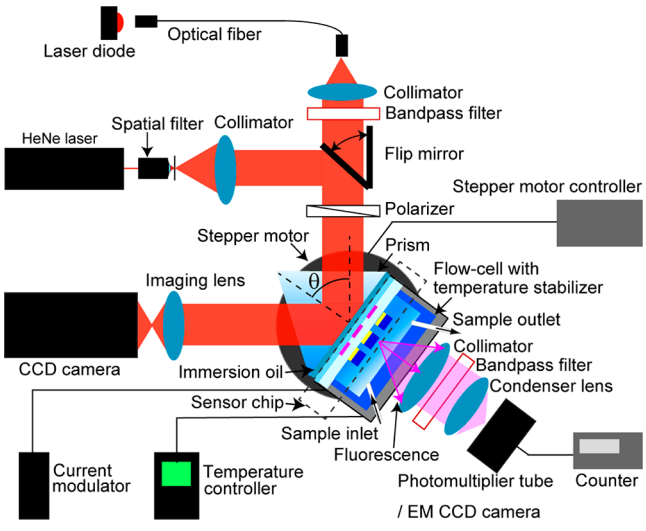

Figure 3. Optical setup employed for the spectroscopy of LRSP and HOW modes that was combined with SPR imaging and surface-plasmon-enhanced fluorescence spectroscopy.

3. RESULTS AND DISCUSSION

3.1. Equilibrium Transition of pNIPAAm Hydrogel. First, an unmodified pNIPAAm hydrogel film with the thickness in a dry state of $d_{h\text{-}dry}$ = 135 nm was attached to the sensor surface, swollen in water, and probed by resonantly excited LRSP and hydrogel optical waveguide (HOW) modes. As Figure 4 shows, the resonant excitation of LRSPs is

dx.doi.org/10.1021/jp400255u | J. Phys. Chem. C 2013, 117, 11705−11712

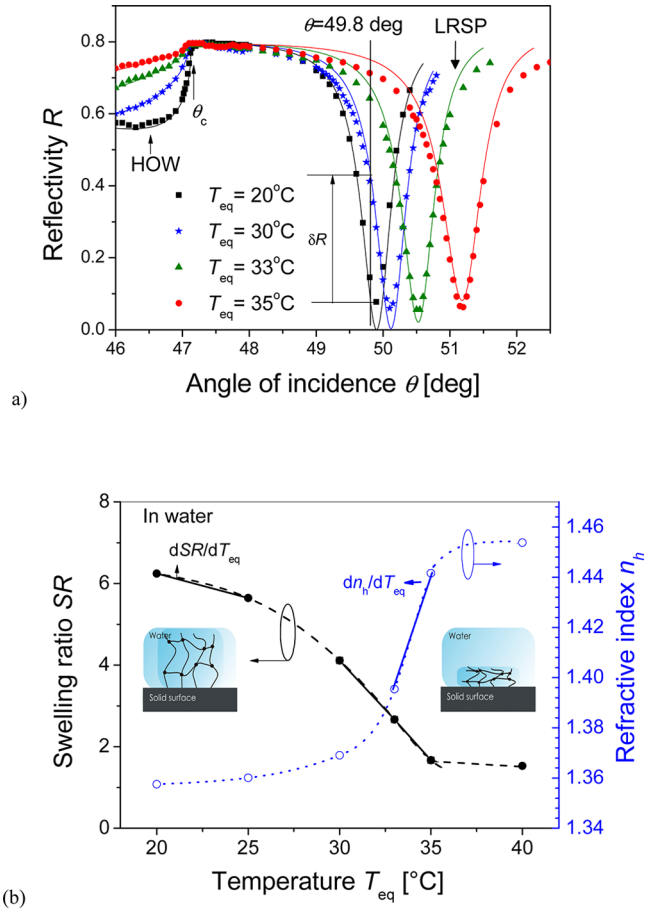

Figure 4. (a) Angular reflectivity spectra measured upon the probing of an unmodified pNIPAAm hydrogel film swollen in water at temperatures T_{eq} = 20, 30, 33, and 35 °C. Lines represent the reflectivity curves fitted by using a Fresnel reflectivity-based model. (b) Respective temperature-dependent equilibrium swelling ratio *SR* and refractive index n_h.

manifested as a narrow dip in the angular reflectivity spectrum located at angles θ = 49.5 to 50.5°. An additional feature is observed below the critical angle $\theta < \theta_c$, which is associated with the appearance of a HOW mode. The hydrogel film gradually collapses as the equilibrium temperature T_{eq} increases, which leads an increase in its refractive index n_h and a decrease in its thickness d_h. These changes are manifested as the shift of the LRSP dip to higher angles θ. In addition, they are accompanied with an increase in reflectivity below the critical angle θ_c as the HOW dip disappears. The swelling ratio *SR* was obtained by dividing the thickness of hydrogel film swollen in water or buffer d_h with that obtained for a dry film $d_{h\text{-}dry}$ in contact with air. Let us note that *SR* is related to the polymer volume fraction $\Phi \propto 1/SR$. Figure 4b shows the temperature-induced variations in swelling ratio *SR* and refractive index n_h of the hydrogel film in contact with water. These data show that swelling ratio *SR* decreases when increasing the temperature T_{eq} and that the *SR* dependence exhibits an inflection point at the LCST = 32 °C for pNIPAAm. The swelling ratio *SR* is 4.1 times higher for the swollen (*SR* = 6.2 at T_{eq} = 20 °C) than that for the collapsed (*SR* = 1.5 at T_{eq} = 40 °C) hydrogel layer, which agrees with previous studies.[22] The transition of the hydrogel between the swollen and the collapsed state is accompanied by a refractive index change as high as $\Delta n_h \approx 0.1$ refractive index units (RIUs). Moreover, this change occurs within a narrow temperature range that translates to a large thermo-optical coefficient of $dn_h/dT \approx 2.2 \times 10^{-2}$ RIU/K at LCST = 32 °C.

Afterward, the equilibrium thermoresponsive properties of pNIPAAm hydrogel film that was modified with mIgG molecules and brought in contact with PBS were investigated. In this set of experiments, the surface mass density Γ of mIgG was adjusted between 0 and 26.4 ng/mm^2, and the unreacted carboxylic groups were passivated by ETA. The surface mass density Γ of immobilized IgG molecules was determined by the spectroscopy of LRSP and HOW modes, as described in previous studies.[12,14] Figure 5 compares the obtained *SR* of

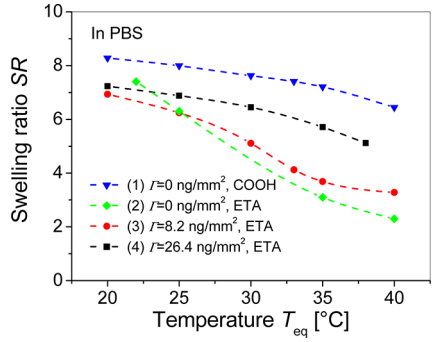

Figure 5. Comparison of the temperature dependence of the equilibrium swelling ratio *SR* for the unmodified hydrogel (triangles), hydrogel modified by ETA (diamonds), and hydrogel decorated with mIgG molecules with surface mass density of Γ = 8.2 (circle) and 26.4 ng/mm^2 (squares) swollen in PBS.

unmodified and modified pNIPAAm hydrogel film in PBS buffer. Interestingly, these data reveal that the unmodified pNIPAAm hydrogel exhibits a higher swelling ratio in PBS than in water; even the osmotic pressure is higher due to the increased salt concentration (e.g., *SR* = 8.3 in PBS and 6.3 in water at T_{eq} = 20 °C). In addition, the thermal responsiveness of the unmodified pNIPAAm is strongly hindered in PBS as its swelling ratio decreases by a factor of only 1.3 when increasing the temperature from T_{eq} = 20 to 40 °C (see curve 1 in Figure 5). Let us note that a similar behavior was observed by atomic force microscopy (AFM) for the pNIPAAm hydrogel films containing carboxylic moieties when they were swollen in Tris buffer.[23] These AFM studies indicated that the increment of buffering agent in a solution leads ionization of carboxylic moieties and enhances solubility of the hydrogel. These effects are accompanied by a shift of the LCST above 32 °C, which is outside the temperature range used in this work. The solubility of the hydrogel film in PBS is suppressed by converting the carboxylic groups to hydroxyl moieties through the modification of MAA with ETA. The ETA-modified pNIPAAm hydrogel in PBS exhibits partially recovered thermoresponsiveness in PBS. When increasing the temperature from T_{eq} = 20 to 40 °C, the swelling ratio of ETA-modified hydrogel decreases by a factor of 2.3. (See curve 2 in Figure 5.) If the carboxylic groups are modified with mIgG, followed by the passivation with ETA, then the strength of a hydrogel collapse gradually decreases as the surface mass density of mIgG increases. As seen in Figure 5 (curves 3 and 4), collapse factors of 2.2 and 1.4 were observed for hydrogel films with mIgG surface mass density of Γ = 8.2 and 26.4 ng/mm^2, respectively. This weak thermoresponsiveness of IgG-modified hydrogel can be attributed to the good solubility of immobilized proteins in

dx.doi.org/10.1021/jp400255u | J. Phys. Chem. C 2013, 117, 11705−11712

the buffer solution. Therefore, the collapse of the hydrogel may be spatially hindered by the presence of (hydrophilic) proteins. This weaker thermally induced collapse of the mIgG-modified hydrogel in contact with PBS is associated with significantly lower thermo-optical coefficient of $dn_h/dT \approx 10^{-3}$ RIU/K at T_{eq} = 32 °C compared with the unmodified hydrogel swollen in water. (See curve 4 in Figure 5.)

3.2. Transition Kinetics of pNIPAAm-Based Hydrogel Films. Kinetics of the swelling and collapse of pNIPAAm hydrogel films was studied by measuring the reflectivity variations upon rapid temperature changes that were induced by applying current to the ITO microheater. First, these kinetics were observed for the unmodified pNIPAAm hydrogel film in contact with water. In this experiment, the background temperature was adjusted to T_0 = 20 °C by using the Peltier element. The angle of incidence was set to θ = 49.8° at the slope of the reflectivity dip that is associated with the coupling to LRSPs; see Figure 4a. The reflectivity signal R was recorded every 20 ms, which is shorter than the response time of the ITO microheater, $\delta t_\mu \approx$ 50 ms. As Figure 6a shows, a stable baseline was first established for the temperature on the surface T_{eq} equal to that of background T_0. Afterward, the current flow I was applied through the microheater at t = 0 for 5 s, which resulted in an increased equilibrium local temperature T_{eq}. The temperature T_{eq} was tuned from 25 to 34 °C by the current I between 5 and 13 mA. The temperature-induced collapse of the hydrogel is manifested as an increase in the measured reflectivity R, which is associated with an increase in the refractive index, n_h, and a decrease in thickness, d_h. When increasing the equilibrium temperature, T_{eq}, the reflectivity R saturates at higher levels due to the stronger collapse of the hydrogel film. Finally, the current flow I was switched off and the local temperature was relaxed back to T_0. This change is accompanied with rapid swelling of the hydrogel and subsequent drop of the reflectivity signal R. The reflectivity changes δR observed on the sensor surface carrying the pNIPAAm hydrogel are of opposite sign and exhibit an order of magnitude higher amplitude than those measured for the bare gold surface in contact with water. (See Figure S1a in Supporting Information.) The reason is that the thermo-optical coefficient of the pNIPAAm hydrogel $dn_h/dT_{eq} = 2.2 \times 10^{-2}$ RIU/K is much larger than that of water $dn_{H_2O}/dT_{eq} = -1.2 \times 10^{-4}$ RIU/K at T_{eq} = 32 °C.

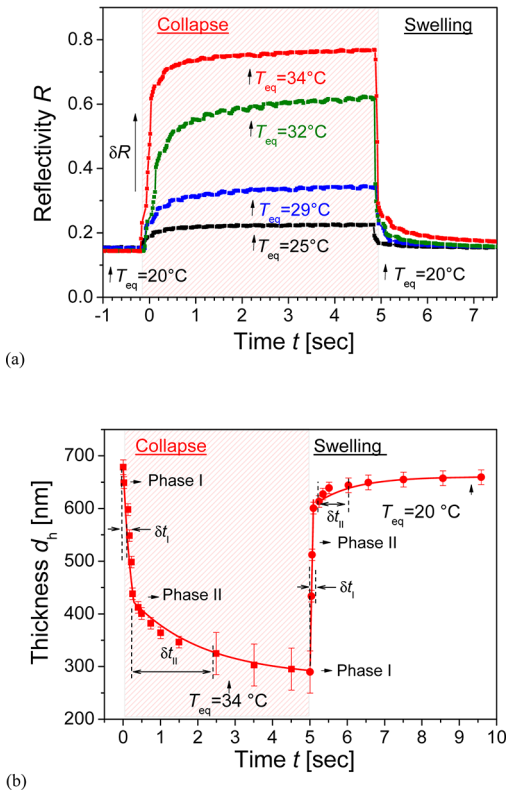

Figure 6. Kinetics of swelling and collapse of unmodified pNIPAAm hydrogel film in contact with water (a) seen from reflectivity changes and (b) respective deconvoluted variations in hydrogel thickness d_h. Current pulses were applied to the ITO microheater to increase the equilibrium temperature between T_{eq} = 25 and 34 °C, and the background temperature was kept at T_0 = 20 °C.

Let us note that variations in the reflectivity signal R due to the temperature-induced detuning of resonant excitation of LRSPs do not change linearly with the hydrogel thickness d_h; see Figure 4a. To obtain more detailed information on the swelling and collapse kinetics, we determined the changes in hydrogel thickness d_h as a function of time by comparing the reflectivity signal R in Figure 6a to a series of angular spectra in Figure 4a that were measured and fitted at different equilibrium temperatures T_{eq}. An example in Figure 6b shows that the swelling of the hydrogel layer occurs in a shorter time than the collapse process. In addition, one can see that the swelling and the collapse proceed in two different phases. In the initial phase of the collapse process, the thickness of the hydrogel rapidly decreases from d_h = 690 to ~400 nm with a characteristic time of $\delta t_I \approx$ 100 ms (phase I). Subsequently, the hydrogel reaches the equilibrium thickness of d_h = 290 nm through a much slower transition with a characteristic time of $\delta t_{II} \approx$ 1 s (phase II). Compared with the collapse process, the initial swelling (phase I) proceeds faster in $\delta t_I \approx$ 50 ms (which is close to the response time of used ITO microheater δt_μ). The following slower phase II is less pronounced and exhibits a characteristic time of $\delta t_{II} \approx$ 1 s. The rapid phase I of the swelling and collapse is probably associated with the fast diffusion of water in and out of the polymer network. The slower phase II observed upon the collapsing of the hydrogel can be attributed to hindered diffusion of water through a dense polymer network and to the possible slow rearrangement of polymer chains in the crowded environment of densely packed chains.[24] The swelling phase II is probably associated with a slow process in which equilibrium between forces driving the swelling and counter-acting strain is established. The polymers used in this study contain three types of monomers (NIPAAm, MAA, and MABP) with different polarity. In particular, the benzophenone groups of the photo-cross-linker monomer MABP are highly apolar and are expected to aggregate during collapse as the polymer density increases and these MABP groups come closer. Upon swelling, the fast kinetics relates to rehydration of the pNIPAAm chains with MAA groups, which generates strain on the network and the hydrophobic aggregates. These aggregates may then slowly restructure and dissolve under the strain of the swollen network, leading to a slow dynamics observed in phase II. Let us note that the difference in the kinetics of swelling and collapse can be also partially ascribed to different slopes dSR/dT_{eq} at the temperature where the hydrogel is swollen ($dSR/dT_{eq} = -0.12$ K^{-1} at T_{eq} = 22.5 °C) and collapsed ($dSR/dT_{eq} = -0.49$ K^{-1} at T_{eq} = 32 °C).

dx.doi.org/10.1021/jp400255u | J. Phys. Chem. C 2013, 117, 11705−11712

Assuming that the initial phase of hydrogel transition between swollen and collapsed state is dominated by 1D Fickian diffusion, its response time to an external stimulus can be described as $\delta t_I \approx d_h^2/2D_m$ (where D_m is a mutual diffusion coefficient). For the hydrogel film with a thickness of d_h = 690 nm and the response time $\delta t_I \approx$ 100 ms, this equation predicts the mutual diffusion coefficient D_m of $\sim 4 \times 10^{-6}$ mm^2 s^{-1}, which is within the lower range of values reported for comparable hydrogel films by other works.[25] For similar NIPAAm-based cross-linked network with the swelling ratio $SR \approx 10$ at room temperature, the cooperative diffusion coefficient of polymer chains $D_{coop} \approx 4 \times 10^{-5}$ mm^2 s^{-1} was measured in ethanol by dynamic light scattering.[24] This value is an order of magnitude higher than the estimated lower limit of D_m, which indicates that swelling and collapse of investigated polymer network is probably faster than the time resolution of developed microheater system. The kinetics of swelling and collapse of the IgG-modified hydrogel film in contact with PBS exhibited similar response times as the unmodified pNIPAAm hydrogel in contact with water. (See the Supporting Information.) Let us note that the swelling and collapse of the hydrogel film was fully reversible. Figure 7 presents an example of the kinetics of reflectivity signal upon periodic series of 100 ms current pulses applied to the ITO microheater with mIgG-modified hydrogel in contact with PBS on its top. The swelling and collapse process of the hydrogel film was highly reproducible for several hundreds of cycles, and the reflectivity peak width of $\Delta t \approx$ 100 ms (defined as full width at half-maximum (fwhm)) was similar to that of the current pulses.

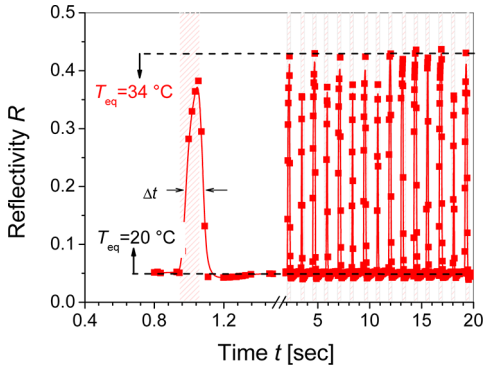

Figure 7. Reflectivity response to series of temperature pulses on the sensor surface with NIPAAm-based hydrogel modified with mIgG and swollen PBS. Current pulses with the magnitude of 14 mA were applied with 2 s interval, and the background temperature was set to T_0 = 20 °C.

3.3. Concept of a Surface Plasmon-Enhanced Fluorescence Biosensor. The presented approach for rapid tuning of SPR can provide new functionalities in biosensors relying on probing the sensor surface with resonantly excited surface plasmons. We show an example in which the detuning of SPR allows for modulating of fluorescence signal in assays that employ surface plasmon-amplified excitation of fluorescence light. In this experiment, a thermoresponsive pNIPAAm hydrogel film (with a thickness of d_h = 860 nm at T_{eq}= 20 °C) was attached to a gold surface with an embedded microheater. The hydrogel polymer network was modified with mIgG by the amine coupling strategy, followed by the affinity capture of a-mIgG (representing a target analyte) that was labeled with Alexa Fluor 647 dyes. The surface mass densities of mIgG and a-mIgG inside the hydrogel network were determined as Γ = 19 and 3.3 ng/mm^2, respectively, by fitting of the respective reflectivity spectra. As Figure 8a reveals, the binding of a-mIgG is manifested by a strong fluorescence signal F occurring at resonance angles where the coupling to HOW and LRSP modes occurs. The reason is that the excitation of such surface waves provides an enhanced electric field intensity that increases the excitation rate of fluorophore labels in the pNIPAAm binding matrix. When the local temperature increases from T_{eq} = 23 to 35 °C, the resonance angles and the respective fluorescence peaks associated with coupling to HOW and LRSP modes shift; see Figure 8b.

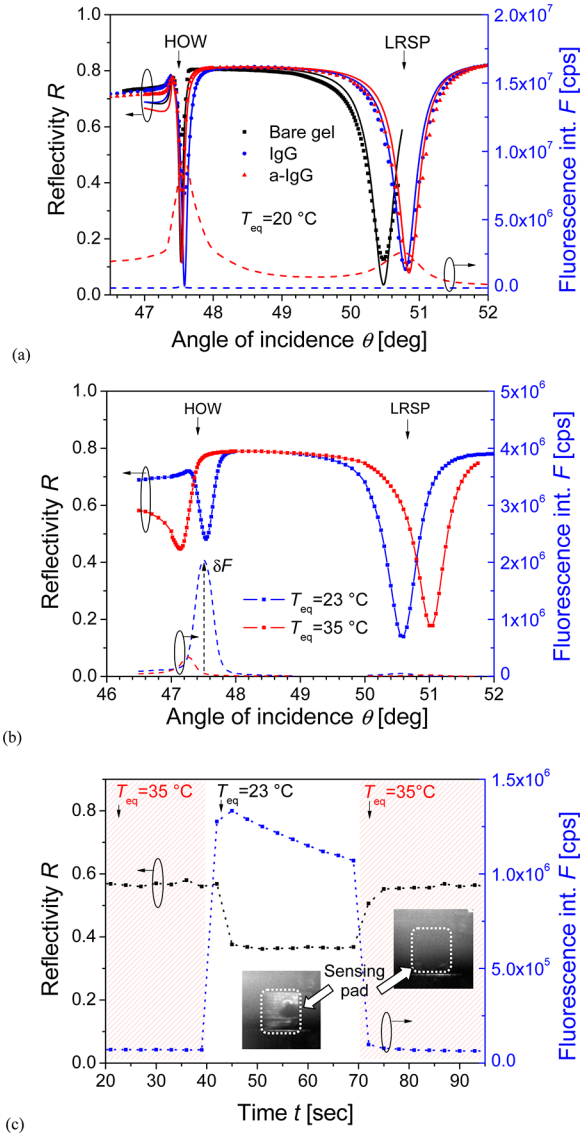

Figure 8. Angular reflectivity and fluorescence spectra for pNIPAAm hydrogel film modified with mIgG (a) before and after the capture of labeled a-mIgG at T_{eq} = 20 °C and (b) after the subsequent change of the equilibrium temperature to T_{eq} = 23 and 35 °C. (c) Time evolution of reflectivity R and fluorescence intensity F upon switching the excitation of HOW at an angle of 47.5° on and off by changing current flow I. Inserted pictures show the respective fluorescence images of sensor spot. (The angular spectra were taken from different sensing areas on the same sensor chip, which caused differences in the fluorescence intensities presented in panels a–c.)

dx.doi.org/10.1021/jp400255u | J. Phys. Chem. C 2013, 117, 11705–11712

Therefore, the fluorescence signal excited with HOW or LRSP optical waves at respective resonant angles of incidence can be virtually switched on and off by swelling and collapse of the hydrogel binding matrix. In further kinetics measurements, we set the incident angle at θ = 47.5°, where the excitation by HOW mode occurs at T_{eq} = 23 °C. As seen in Figure 8c, the sensor surface was first operated at T_{eq} = 35 °C for which the coupling to HOW does not occur and thus only weak fluorescence signal F is observed. After switching off the ITO microheater to cool the surface to T_{eq} = 23 °C, the reflectivity signal R drops, which indicates a stronger coupling to HOW modes and results in the occurrence of a strong fluorescence signal F. When switching the temperature back to T_{eq} = 35 °C, the reflectivity increases to original level and the fluorescence signal drops back to the background. Let us note that the gradual decrease in the signal after switching the excitation field on is probably due to bleaching of the fluorescent dyes. The inserted images in Figure 8c show the spatial distribution of the fluorescence signal from a sensing spot that was observed by an EM-CCD camera. Upon coupling to the HOW mode for T_{eq} = 23 °C, a clear fluorescence signal from the functionalized pad is observed. After increasing the temperature to T_{eq} = 35 °C, the fluorescence signal decreases to the background level and the bright pad disappears.

4. CONCLUSIONS

A new concept for rapid tuning of SPR in advanced biosensor applications is presented. This approach is based on a sensor chip with a metallic layer, thermoresponsive pNIPAAm hydrogel film, and an embedded ITO microheater. The reversible swelling and collapse of the hydrogel film allows for strong variations of refractive index on the metallic sensor surface due to the large pNIPAAm thermo-optical coefficient. The swelling and collapse occur with a characteristic response time below 100 ms, are fully reversible, and depend on the hydrogel postmodification and on the swelling buffer. The used pNIPAAm-based hydrogel system is particularly attractive for biosensor applications because it can simultaneously serve as a large binding-capacity matrix for the specific capture of molecular analytes. An example of possible application in a surface plasmon-enhanced fluorescence biosensing is presented. We show that rapid switching on and off the surface plasmon-enhanced field intensity allows us to efficiently tune the excitation strength of fluorescence light. Among others, this functionality holds potential for multiplexing of sensing channels through sequential readout of the fluorescence signal emitted from different spatially separated sensing spots.

■ ASSOCIATED CONTENT

Supporting Information

Calibration of microheaters embedded in SPR sensor chips with data showing the kinetics of swelling and collapsing of pNIPAAm-based hydrogel film that was functionalized with IgG molecules. Description of determining the thickness of hydrogel thin films d_h based on the analysis of reflectivity spectrum with LRSP and HOW resonances. This material is available free of charge via the Internet at http://pubs.acs.org.

■ AUTHOR INFORMATION

Corresponding Author

*E-mail: jakub.dostalek@ait.ac.at. Tel: +43 (0) 50550 4470. Fax: +43(0) 50550-4450.

Notes

The authors declare no competing financial interest.

■ ACKNOWLEDGMENTS

We acknowledge the partial support for this work provided by Austrian Science Fund (FWF) through the project ACTIPLAS (P 244920-N20) and the European Soft Matter Infrastructure project (ESMI), FP7-INFRASTRUCTURES-2010-1, Grant Agreement Number 262348 of the European Commission.

■ REFERENCES

(1) Schuller, J. A.; Barnard, E. S.; Cai, W. S.; Jun, Y. C.; White, J. S.; Brongersma, M. L. Plasmonics for Extreme Light Concentration and Manipulation. *Nat. Mater.* **2010**, *9*, 193−204.

(2) (a) Dicken, M. J.; Sweatlock, L. A.; Pacifici, D.; Lezec, H. J.; Bhattacharya, K.; Atwater, H. A. Electrooptic Modulation in Thin Film Barium Titanate Plasmonic Interferometers. *Nano Lett.* **2008**, *8*, 4048−4052. (b) Smalley, J. S. T.; Zhao, Y. H.; Nawaz, A. A.; Hao, Q. Z.; Ma, Y.; Khoo, I. C.; Huang, T. J. High Contrast Modulation of Plasmonic Signals Using Nanoscale Dual-Frequency Liquid Crystals. *Opt. Express* **2011**, *19*, 15265−15274.

(3) Gagnon, G.; Lahoud, N.; Mattiussi, G. A.; Berini, P. Thermally Activated Variable Attenuation of Long-Range Surface Plasmon-Polariton Waves. *J. Lightwave Technol.* **2006**, *24*, 4391−4402.

(4) Temnov, V. V.; Armelles, G.; Woggon, U.; Guzatov, D.; Cebollada, A.; Garcia-Martin, A.; Garcia-Martin, J. M.; Thomay, T.; Leitenstorfer, A.; Bratschitsch, R. Active Magneto-Plasmonics in Hybrid Metal-Ferromagnet Structures. *Nat. Photonics* **2010**, *4*, 107−111.

(5) Chen, H. S.; Wang, J. Y.; Yeh, S. S.; Chen, C. D.; Lin, H. Y. Modulation of Surface Plasmon Wave by Photo-Induced Refractive Index Changes of CdSe Quantum Dots *Appl. Phys. Lett.* **2012**, *100*.

(6) Leroux, Y.; Lacroix, J. C.; Fave, C.; Trippe, G.; Felidj, N.; Aubard, J.; Hohenau, A.; Krenn, J. R. Tunable Electrochemical Switch of the Optical Properties of Metallic Nanoparticles. *ACS Nano* **2008**, *2*, 728−732.

(7) (a) Coppola, G.; Sirleto, L.; Rendina, I.; Iodice, M. Advance in Thermo-Optical Switches: Principles, Materials, Design, and Device Structure *Opt. Eng.* **2011**, *50*; (b) Zhang, X. Y.; Zhang, T.; Hu, A. M.; Xue, X. J.; Wu, P. Q.; Chen, Q. Y. Tunable Microring Resonator Based on Dielectric-Loaded Surface Plasmon Polariton Waveguides. *J. Nanosci. Nanotechnol.* **2011**, *11*, 10520−10524.

(8) Kuckling, D.; Harmon, M. E.; Frank, C. W. Photo-Cross-Linkable PNIPAAm Copolymers. 1. Synthesis and Characterization of Constrained Temperature-Responsive Hydrogel Layers. *Macromolecules* **2002**, *35*, 6377−6383.

(9) (a) Tokareva, I.; Minko, S.; Fendler, J. H.; Hutter, E. Nanosensors Based on Responsive Polymer Brushes and Gold Nanoparticle Enhanced Transmission Surface Plasmon Resonance Spectroscopy. *J. Am. Chem. Soc.* **2004**, *126*, 15950−15951. (b) Gehan, H.; Mangeney, C.; Aubard, J.; Levi, G.; Hohenau, A.; Krenn, J. R.; Lacaze, E.; Felidj, N. Design and Optical Properties of Active Polymer-Coated Plasmonic Nanostructures. *J. Phys. Chem. Lett.* **2011**, *2*, 926−931.

(10) Gehan, H.; Fillaud, L.; Chehimi, M. M.; Aubard, J.; Hohenau, A.; Felidj, N.; Mangeney, C. Thermo-Induced Electromagnetic Coupling in Gold/Polymer Hybrid Plasmonic Structures Probed by Surface-Enhanced Raman Scattering. *ACS Nano* **2010**, *4*, 6491−6500.

(11) Beines, P. W.; Klosterkamp, I.; Menges, B.; Jonas, U.; Knoll, W. Responsive Thin Hydrogel Layers from Photo-Cross-Linkable Poly-(N-isopropylacrylamide) Terpolymers. *Langmuir* **2007**, *23*, 2231−2238.

(12) Aulasevich, A.; Roskamp, R. F.; Jonas, U.; Menges, B.; Dostalek, J.; Knoll, W. Optical Waveguide Spectroscopy for the Investigation of Protein-Funcionalized Hydrogel Films. *Macromol. Rapid Commun.* **2009**, *30*, 872−877.

(13) Wang, Y.; Huang, C. J.; Jonas, U.; Dostalek, J.; Knoll, W. Biosensor Based on Hydrogel Optical Waveguide Spectroscopy. *Biosens. Bioelectron.* **2010**, *25*, 1663−1668.
(14) Wang, Y.; Brunsen, A.; Jonas, U.; Dostalek, J.; Knoll, W. Prostate Specific Antigen Biosensor Based on Long Range Surface Plasmon-Enhanced Fluorescence Spectroscopy and Dextran Hydrogel Binding Matrix. *Anal. Chem.* **2009**, *81*, 9625−9632.
(15) Huang, C. J.; Dostalek, J.; Knoll, W. Long Range Surface Plasmon and Hydrogel Optical Waveguide Field-Enhanced Fluorescence Biosensor with 3D Hydrogel Binding Matrix: On the Role of Diffusion Mass Transfer. *Biosens. Bioelectron.* **2010**, *26*, 1425−1431.
(16) (a) Junk, M. J. N.; Anac, I.; Menges, B.; Jonas, U. Analysis of Optical Gradient Profiles during Temperature- and Salt-Dependent Swelling of Thin Responsive Hydrogel Films. *Langmuir* **2010**, *26*, 12253−12259. (b) Yu, H.; Grainger, D. W. Thermosensitive Swelling Behavior in Cross-Linked N-Isopropylacrylamide Networks - Cationic, Anionic, and Ampholytic Hydrogels. *J. Appl. Polym. Sci.* **1993**, *49*, 1553−1563. (c) van den Brom, C. R.; Anac, I.; Roskamp, R. F.; Retsch, M.; Jonas, U.; Menges, B.; Preece, J. A. The Swelling Behaviour of Thermoresponsive Hydrogel/Silica Nanoparticle Composites. *J. Mater. Chem.* **2010**, *20*, 4827−4839.
(17) Anac, I.; Aulasevich, A.; Junk, M. J. N.; Jakubowicz, P.; Roskamp, R. F.; Menges, B.; Jonas, U.; Knoll, W. Optical Characterization of Co-Nonsolvency Effects in Thin Responsive PNIPAAm-Based Gel Layers Exposed to Ethanol/Water Mixtures. *Macromol. Chem. Phys.* **2010**, *211*, 1018−1025.
(18) Gee, K. R.; Archer, E. A.; Kang, H. C. 4-Sulfotetrafluorophenyl (STP) Esters: New Water-Soluble Amine-Reactive Reagents for Labeling Biomolecules. *Tetrahedron Lett.* **1999**, *40*, 1471−1474.
(19) Junk, M. J. N.; Jonas, U.; Hinderberger, D. EPR Spectroscopy Reveals Nanoinhomogeneities in the Structure and Reactivity of Thermoresponsive Hydrogels. *Small* **2008**, *4*, 1485−1493.
(20) Dostalek, J.; Kasry, A.; Knoll, W. Long Range Surface Plasmons for Observation of Biomolecular Binding Events at Metallic Surfaces. *Plasmonics* **2007**, *2*, 97−106.
(21) Huang, C. J.; Dostalek, J.; Knoll, W. Optimization of Layer Structure Supporting Long Range Surface Plasmons for Surface Plasmon-Enhanced Fluorescence Spectroscopy Biosensors. *J. Vac. Sci. Technol., B* **2010**, *28*, 66−72.
(22) Anac, I.; Aulasevich, A.; Junk, M. J. N.; Jakubowicz, P.; Roskamp, R. F.; Menges, B.; Jonas, U.; Knoll, W. Optical Characterization of Co-Nonsolvency Effects in Thin Responsive PNIPAAm-Based Gel Layers Exposed to Ethanol/Water Mixtures *Macromol. Chem. Phys. 211*, 1018-1025.
(23) Melzak, K. A.; Mateescu, A.; Toca-Herrera, J. L.; Jonas, U. Simultaneous Measurement of Mechanical and Surface Properties in Thermoresponsive, Anchored Hydrogel Films. *Langmuir* **2012**, *28*, 12871−12878.
(24) Gianneli, M.; Roskamp, R. F.; Jonas, U.; Loppinet, B.; Fytas, G.; Knoll, W. Dynamics of Swollen Gel Layers Anchored to Solid Surfaces. *Soft Matter* **2008**, *4*, 1443−1447.
(25) Singh, J.; Weber, M. E. Kinetics of One-Dimensional Gel Swelling and Collapse for Large Volume Changes. *Chem. Eng. Sci.* **1996**, *51*, 4499−4608.